Atomic data for opacity calculations: XVIII. Photoionization and oscillator strengths of Si-like ions Si^0, S^{2+}, Ar^{4+}, Ca^{6+}

Sultana N Nahar and Anil K Pradhan

Department of Astronomy, The Ohio State University, Columbus, OH 43210, USA

Abstract. Photoionization cross sections, oscillator strengths and energy levels of the silicon-like ions, Si^0, S^{2+}, Ar^4 and Ca^{6+} are calculated in the close coupling approximation using the R-matrix method. A large number of bound states with $n \leqslant 10$ have been considered and oscillator strengths for transitions among all these states and photoionization cross sections of all the bound states are obtained. Partial photoionization cross sections of the ground state into various excited states of the residual ion are also obtained for each ion. Detailed comparisons have been made for the calculated energies, oscillator strengths and photoionization cross sections with available theoretical and experimental values. Whereas we find good agreement for the oscillator strengths with recent experimental data for Si^0 and S^{2+}, there are very few previous data available for Ar^{4+} and Ca^{6+}. The ground-state photoionization cross sections for Si^0 agree well with the previous close coupling calculations, however the present R-matrix results show considerable differences from the background cross sections for Si^0, S^{2+} and Ar^{4+} in the central field approximations.

1. Introduction

A description of the aim of the Opacity Project (OP) and the calculations of accurate atomic radiative data in the close coupling (CC) approximation using the R-matrix method is given by Seaton (1987) and Berrington *et al* (1987) in the atomic data for opacity calculations (ADOC) series. The radiative data include energy levels, oscillator strengths and photoionization cross sections for nearly all astrophysically abundant atoms and ions ions that contribute to stellar opacities. Several of these results have been reported in previous papers in the ADOC series.

With a few exceptions for heavy atomic systems that are treated individually, the ADOC calculations are usually carried out along isoelectronic sequences since the primary characteristics of the atomic eigenfunction expansions, and corresponding computations, remain the same along the sequence so long as relativistic effects are not considered. States belonging to the ground complex of configurations are usually retained in the CC expansion. While this criterion serves well for sequences that are isoelectronic with the second row of elements of the periodic table, and enables the same set of eigenstates to be employed in the CC calculations for all ions in a given sequence, it is found that for the third row sequences the situation is more complicated and different eigenfunction expansions need to be employed for different ions. In the present work we present the first results for a third row sequence. Details are discussed in section 3.

Relatively sparse calculations have previously been reported for some Si-sequence ions, such as the ground state photoionization cross sections of Si^0 (Mendoza and

Zeippen 1988), dipole oscillator strengths for a small number of strong transitions in Si^0 (Mendoza and Zeippen 1988) and S^{2+} (Ho and Henry 1987), and a number of fine structure transitions in Ar^{6+} (Biemont 1986). The present calculations are comprehensive; they include all bound states with $n \leq 10$ and $l \leq 5$, and amount to a few hundred excited states for each atom and ion. Photoionization cross sections for all bound states, and dipole oscillator strengths in length and velocity formulations for all transitions, have been calculated. In the present paper we describe the computations and some of the important results and associated features. Detailed comparisons are made with available experimental and theoretical data.

2. Theoretical framework

In analogy with collisional work where the N-electron 'target' ion is represented by a coupled eigenfunction expansion in terms of the included target states, in the radiative work we similarly represent the 'core' ion or the 'residual' ion, as in the case of photoionization. The total $(e + ion)$ system is then expanded in terms of the N-electron target wavefunctions given by

$$\Psi^{SL\pi}(E) = A \sum_{i=1}^{I} \chi_i(r^{-1})\theta_i + \sum_{j=1}^{J} c_j \Phi_j \tag{1}$$

where $\chi_i(r^{-1})$ are the target states

$$\chi_i(x) = \chi(\Gamma_i L_i S_i M_{L_i} M_{S_i} \pi_i | x)$$

$x = r^{-1}$ represents all the coordinates of the N-electron system that do not include r, and θ_i are the free electron wavefunctions with a radial part $F_i(r)$. A denotes the antisymmetrization operator. The second sum consists of square-integrable correlation type function Φ_j, that have the form of bound states of the $(N + 1)$-electron system, with variational parameters c_j. The second sum represents the constraint on $F_i(r)$ requiring its orthogonality to the target orbitals of the same symmetry, and may also include the short range correlation effects. I is the number of target states which corresponds to the number of 'free' channels and J is the number of 'bound' channels in the cc expansion of the $(N + 1)$-electron wavefunction Ψ for a given symmetry $SL\pi$ at total energy E.

The bound- and continuum-state wavefunctions can be obtained for $E < 0$ and for $E \geq 0$ employing the R-matrix method as explained by Berrington *et al* (1987). With the bound and the continuum $(e + ion)$ states thus given by equation (1), we may obtain both the bound–bound radiative transition probabilities, or the oscillator strengths, as

$$f(b, a) = \frac{\Delta E}{3g_a} S(b; a) \tag{2}$$

and the bound–free photoionization cross sections as

$$\sigma_{PI} = \frac{4\pi^2 a_0^2 \alpha}{3} E_\omega \frac{S(b, a)}{g_a} \tag{3}$$

where $\Delta E = E_b - E_a$ is the energy difference, in Rydbergs, between states b and a, E_ω is the photon energy, and g_a is the statistical weight factor of the initial state. $S(b, a)$

is the line strength given by

$$S(b, a) = |(b\|D\|a)|^2 \qquad (4)$$

where D is the dipole operator. More complete theoretical details are given by Seaton (1987) and Yu and Seaton (1987).

3. Computations

3.1. Target states: energies and oscillator strengths

The target states considered for each ion of the Si sequence are given in table 1. The N-electron basis set is represented by an eight-state expansion for Si^+, 16-state for S^{3+}, thirteen-state for Ar^{5+} and eighteen-state for Ca^{7+}. The wavefunction expansions of Si^+ and S^{3+} include some states dominated by the $n = 4$ complex, but for Ar^{5+} and Ca^{7+} only the states from the $n = 3$ complex are included as the $n = 4$ states are energetically too high to be of interest. An updated version of the SUPERSTRUCTURE program (Eissner *et al* 1974) is used to generate the target orbitals that are optimized with configuration interaction (CI) type target state wavefunctions. The CI target expansion consists of two sets of configurations: *spectroscopic* configurations that dominate the included target states and *correlation* configurations that are included for CI only, and not in the eigenfunction expansion. One important criterion in determination of the CI expansion for the target states is to optimize the expansion so as to avoid pesudoresonances in photoionization cross sections. SUPERSTRUCTURE employs a scaled Thomas–Fermi–Dirac potential to obtain the one-electron orbitals; the scaling parameter λ and the spectroscopic and correlation configurations for each ion are listed in table 1.

Comparison is made in table 1 of the calculated and observed target energies relative to the ground state $3s^23p(^2P^o)$ energy. The present calculated energies compare well with the observed energies; the largest difference is less than 6% for all the ions.

A more sensitive indicator of the accuracy of the target state wavefunctions is in the oscillator strengths, or f-values, for dipole allowed transitions within the target. The f-values are presented and compared with available observed and calculated values in table 2. We compare the present calculated f-values in the length from. Comparison of Si^+ oscillator strengths shows that, except for the transitions $3s^23p\ ^2P^o-3s3p^2(^2D, ^2S)$, the present f_L values are within 5% of very accurate calculated values of Luo *et al* (1988), who employed a large CI expansion in their calculations optimized for a few selected transitions. The agreement with the experimentally measured values is also found to be good.

For the target ions S^{3+}, Ar^{5+} and Ca^{7+} we compare with the most accurate previous theoretical values, which are from the OP calculations for the Al-sequence ions (Mendoza *et al* 1992). In the case of S^{3+}, present f_L values are within 8% of the OP values by Mendoza *et al*. Both the present and the Mendoza *et al* values agree reasonably well with the experimental values. Similarly for Ar^{5+} the present values and the Mendoza *et al* values agree well (except for the transition $3s3p^2\ ^4P-3p3d\ ^4P^o$), and both agree better with the measured values of Livingston *et al* (1976) than with those of Morton (1978). Oscillator strengths of Ca^{7+} in the present work and that of Mendoza *et al* differ by less than 8%, except for the transitions $3s^23p\ ^2P^o-3s3p^2\ ^2D$ and $3s3p^2\ ^4P-3p3d\ ^4D^o$. In general we find that the target data for the ions considered, energies and oscillator strengths, compare reasonably well with previously available data, usually

Table 1. Target states (eight for Si$^+$, 16 for S^{3+}, 13 for Ar^{5+}, and 18 for Ca^{7+}) for the CC expansions and comparison of their calculated energy values (cal.) with the observed ones (obs). The observed energies are from Martin and Zalubas (1983) for Si$^+$, Martin *et al* (1990) for S^{3+}, Kelly (1987) for Ar^{5+} and Sugar and Corliss (1985) for Ca^{7+}. The spectroscopic and correlation configurations in the eigenfunction expansion of these target ions and the values of scaling parameter λ in Thomas–Fermi potential are given below. A bar on an orbital represents correlation orbital.

State	cal	obs	State	cal	obs	State	cal	obs
				Si$^+$				
3s^{2}3p ^{2}P$^{\circ}$	0	0.001 74	3s^{2}4s ^{2}S	0.611 93	0.596 88	3s^{2}4p ^{2}P$^{\circ}$	0.762 41	0.740 23
3s3p^2 ^{4}P	0.369 19	0.391 86	3s3p^2 ^{2}S	0.713 98	0.698 63	3s3p^2 ^{2}P	0.776 60	0.764 89
3s3p^2 ^{2}D	0.503 02	0.504 10	3s^{2}3d ^{2}D	0.741 80	0.723 08			
				S^{3+}				
3s^{2}3p ^{2}P$^{\circ}$	0	0.000 69	3s^{2}4s ^{2}S	1.654 96	1.653 48	3s3p ^{3}P$^{\circ}$ 3d ^{4}P$^{\circ}$	2.016 19	2.026 45
3s3p^2 ^{4}P	0.624 56	0.653 78	3p^3 ^{2}D$^{\circ}$	1.656 11	1.686 85	3s3p ^{3}P$^{\circ}$ 3d ^{4}D$^{\circ}$	2.046 40	2.046 07
3s3p^2 ^{2}D	0.844 84	0.857 79	3p^3 ^{4}S$^{\circ}$	1.794 46	1.790 23	3s3p ^{3}P$^{\circ}$ 3d ^{2}D$^{\circ}$	2.185 63	2.128 93
3s3p^2 ^{2}S	1.195 77	1.125 50	3s3p ^{3}P$^{\circ}$ 3d ^{4}F$^{\circ}$	1.835 82	1.858 16	3s3p ^{3}P$^{\circ}$ 3d ^{2}F$^{\circ}$	2.254 60	2.206 08
3s3p^2 ^{2}P	1.232 28	1.221 43	3p^3 ^{2}P$^{\circ}$	1.940 55	1.926 14			
3s^{2}3d ^{2}D	1.432 58	1.386 41	3s^{2}4p ^{2}P$^{\circ}$	1.964 73	1.946 97			
				Ar^{5+}				
3s^{2}3p ^{2}P$^{\circ}$	0	0.013 41	3s^{2}3d ^{2}D	2.0480	1.992 31	3s3p ^{3}P$^{\circ}$ 3d ^{4}P$^{\circ}$	2.867 7	2.886 39
3s3p^2 ^{4}P	0.8758	0.924 40	3p^3 ^{2}D$^{\circ}$	2.3215		3s3p ^{3}P$^{\circ}$ 3d ^{4}D$^{\circ}$	2.905 8	2.913 60
3s3p^2 ^{2}D	1.1810	1.207 72	3p^3 ^{4}S$^{\circ}$	2.4552	2.465 10	3s3p ^{3}P$^{\circ}$ 3d ^{2}D$^{\circ}$	3.066 4	
3s3p^2 ^{2}S	1.6306	1.547 34	3s3p ^{3}P$^{\circ}$ 3d ^{4}F$^{\circ}$	2.6260				
3s3p^2 ^{2}P	1.6687	1.668 64	3p^3 ^{2}P$^{\circ}$	2.7032				
				Ca^{7+}				
3s^{2}3p ^{2}P$^{\circ}$	0	0.026 17	3p^3 ^{2}D$^{\circ}$	2.968 89		3s3p ^{3}P$^{\circ}$ 3d ^{2}D$^{\circ}$	3.899 82	
3s3p^2 ^{4}P	1.126 90	1.199 20	3p^3 ^{4}S$^{\circ}$	3.102 19	3.146 37	3s3p ^{3}P$^{\circ}$ 3d ^{2}F$^{\circ}$	4.093 74	
3s3p^2 ^{2}D	1.508 16	1.564 89	3s3p ^{3}P$^{\circ}$ 3d ^{4}F$^{\circ}$	3.386 48		3x3p ^{3}P$^{\circ}$ 3d ^{2}P$^{\circ}$	4.467 35	
3s3p^2 ^{2}S	2.040 04	1.973 67	3p^3 ^{2}P$^{\circ}$	3.422 01		3s3p ^{1}P$^{\circ}$ 3d ^{2}F$^{\circ}$	4.569 92	
3s3p^2 ^{2}P	2.090 47	2.120 83	3s3p ^{3}P$^{\circ}$ 3d ^{4}P$^{\circ}$	3.683 29	3.723 92	3s3p ^{1}P$^{\circ}$ 3d ^{2}D$^{\circ}$	4.777 34	
3s^{2}3d ^{2}D	2.616 50	2.574 23	3s3p ^{3}P$^{\circ}$ 3d ^{4}D$^{\circ}$	3.723 86	3.760 28	3s3p ^{1}P$^{\circ}$ 3d ^{2}P$^{\circ}$	4.789 40	

Si$^+$: Spectroscopic: 3s^{2}3p, 3s3p^2, 3s^{2}3d, 3s^{2}4s, 3s^{2}4p
Correlation: 3s^{2}4d, 3s3p3d, 3s3p4s, 3s3p4p, 3s3p4d, 3s3d4s, 3s3d4p, 3s3d4d, 3s3d4f, 3p^3, 3p^{2}3d, 3p^{2}4s, 3p^{2}4p, 3p^{2}4d, 3p3d4s, 3p3d4p, 3p3d4d, 3p3d4f, 3p3d^2, 3d^3
$\underline{\lambda}$: 1.0874 (1s), 1.0874 (2s), 1.0154 (2p), 1.0449 (3s), 1.03591 (3p), 1.18176 (3d), 1.1114 (4s), 1.1515 (4p), 1.50001 ($\overline{4d}$), 2.99166 ($\overline{4f}$)

S^{3+}: Spectroscopic: 3s^{2}3p, 3s3p^2, 3p^3, 3s^{2}3d, 3s3p3d, 3s^{2}4s, 3s^{2}4p
Correlation: 3s^{2}4d, 3s3p4s, 3s3p4p, 3s3p4d, 3s3d4s, 3s3d4p, 3s3d4d, 3p^{2}3d, 3p^{2}4s, 3p^{2}4p, 3p^{2}4d, 3p3d4s, 3p3d4p, 3p3d4d
$\underline{\lambda}$: 1.1(1s), 1.08576 (2s), 1.03329 (2p), 1.07439 (3s), 1.04779 (3p), 1.03206 (3d), 1.14812 (4s), 1.15514 (4p), 1.42067 ($\overline{4d}$)

Ar^{5+}: Spectroscopic: 3s^{2}3p, 3s3p^2, 3p^3, 3s^{2}3d, 3s3p3d
Correlation: 3s^{2}4s, 3s^{2}4p, 3s3p4s, 3s3p4p, 3s3d4s, 3s3d4p, 3p^{2}3d, 3p^{2}4s, 3p^{2}4p, 3p3d4s, 3p3d4p
$\underline{\lambda}$: 1.1 (1s), 1.08576 (2s), 1.03329 (2p), 0.93817 (3s), 0.96008 (3p), 1.1118 (3d), 2.64572 ($\overline{4s}$), 2.12666 ($\overline{4p}$)

Ca^{7+}: Spectroscopic: 3s^{2}3p, 3s3p^2, 3p^3, 3s^{2}3d, 3s3p3d
Correlation: 3s^{2}4s, 3s^{2}4p, 3s3p4s, 3s3p4p, 3s3d4s, 3s3d4p, 3p^{2}3d, 3p^{2}4s, 3p^{2}4p, 3p3d4s, 3p3d4p
$\underline{\lambda}$: 1.1 (1s), 1.08576 (2s), 1.03329 (2p), 0.9470 (3s), 0.90957 (3p), 1.10689 (3d), 3.25982 ($\overline{4s}$), 2.69876 ($\overline{4p}$)

Table 2. Oscillator strengths of the target ions Si$^+$, S^{3+}, Ar^{5+}, and Ca^{6+}. f_L corresponds to calculated oscillator strengths and 'expt' to measured values. LPS, Luo *et al* (1988).

Transition	f_L (present)	f_L (LPS)	f (expt)
		Si$^+$	
3s^{2}3p ^{2}P$^\circ$–3s3p^2 ^{2}P	0.895	0.880	0.74[a], 0.96[b]
3s^{2}3p ^{2}P$^\circ$–3s^{2}3d ^{2}D	1.103	1.162	1.14[a]
3s^{2}3p ^{2}P$^\circ$–3s3p^2 ^{2}D	0.0015	0.0035	0.0036[b]
3s^{2}4p ^{2}P$^\circ$–3s3p^2 ^{2}D	0.101		0.108[c]
3s^{2}3p ^{2}P$^\circ$–3s3p^2 ^{2}S	0.107	0.091	0.147[b]
3s^{2}3p ^{2}P$^\circ$–3s^{2}4s ^{2}S	0.115	0.118	0.077[b]
3s^{2}4s ^{2}S–3s^{2}4p ^{2}P$^\circ$	1.227		1.185[c]

Transition	(present)	(OP)	(expt)
		S^{3+}	
3s^{2}3p ^{2}P$^\circ$–3s3p^2 ^{2} ^{2}D	0.037	0.048	0.041±0.002[d], 0.035±0.002[e]
3s^{2}3p ^{2}P$^\circ$–3s^{2}3d ^{2}D	1.216	1.183	0.91±0.15[d]
3s3p^2 ^{4}P–3p3d ^{4}D$^\circ$	1.290	1.192	0.92±0.12[d]
3s^{2}3p ^{2}P$^\circ$–3s3p^2 ^{2}P	0.759	0.762	0.56±0.15[d], 1.11±0.15[f]
3s3p^2 ^{4}P–3p^3 ^{4}S$^\circ$	0.258	0.254	0.21±0.03[d]
3s^{2}3p ^{2}P$^\circ$–3s3p^2 ^{2}S	0.104	0.105	0.15±0.02[d], 0.132±0.0005[f]
3s^{2}3p ^{2}P$^\circ$–3p^{2}4s ^{2}S	0.089	0.087	0.096±0.006[f]

Transition	(present)	(OP)	(expt)
		Ar^{5+}	
3s^{2}3p ^{2}P$^\circ$–3s^{2}3d ^{2}D	0.961	0.942	0.667±0.17[g], 0.617±0.07[h]
3s^{2}3p ^{2}P$^\circ$–3s3p^2 ^{2}D	0.054	0.065	0.06±0.005[g], 0.06±0.005[h]
3s^{2}3p ^{2}P$^\circ$–3s3p^2 ^{2}P	0.652	0.655	
3s^{2}3p ^{2}P$^\circ$–3s3p^2 ^{2}S	0.086	0.087	0.067±0.005[g], 0.0617±0.007[h]
3s3p^2 ^{4}P–3p^3 ^{4}S$^\circ$	0.225	0.220	0.152±0.01[h]
3s3p^2 ^{4}P–3p3d ^{4}P$^\circ$	0.403	0.340	
3s3p^2 ^{4}P–3p3d ^{4}D$^\circ$	1.032	0.958	

Transition	(present)	(OP)	(expt)
		Ca^{7+}	
3s^{2}3p ^{2}P$^\circ$–3s3p^2 ^{2}D	0.061	0.070	
3s^{2}3p ^{2}P$^\circ$–3s3p^2 ^{2}S	0.077	0.076	
3s^{2}3p ^{2}P$^\circ$–3s3p^2 ^{2}P	0.567	0.572	
3s^{2}3p ^{2}P$^\circ$–3s^{2}3d ^{2}D	0.781	0.763	
3s3p^2 ^{4}P–3p^3 ^{4}S$^\circ$	0.197	0.194	
3s3p^2 ^{4}P–3p3d ^{4}P$^\circ$	0.328	0.277	
3s3p^2 ^{4}P–3p3d ^{4}D$^\circ$	0.840	0.777	

[a] Livingston *et al* (1976).
[b] Morton (1978).
[c] Shulz-Gulde (1969).
[d] Irwin and Livingston (1976).
[e] Berry *et al* (1970).
[f] Reistad and Enystrom (1988).
[g] Livingston *et al* (1981).
[g] Buchet-Poulizac *et al* (1982).

to within 5-10%, sufficient to ensure accurate eigenfunctions for the CC calculations for the (e+ion) system (described in the following section).

3.2. (N+1)-electron system

The R-matrix package of codes employed for the $(N+1)$ electron system is described by Berrington *et al* (1987). The one-electron target basis set, optimized with SUPER-STRUCTURE, is used to construct target state wavefunctions. The radiative calculations consider free electron angular momenta up to $l \le 5$, which when coupled with the target states $S_t L_t \pi_t$ listed in table 1, yield a large number of bound (e+ion) symmetries $SL\pi = {}^{1,3,5}(S, P, D, F, G, H, I)^{e,o}$ below the first ionization threshold as given in table 3.

Table 3. Total number of $(S_t L_t \pi_t)nl$ bound symmetries ($N_{SL\pi}$), bound states (N_{bnd}) and the range of each bound spin multiplet with $n \le 10$, $l \le 5$ for the Si-like ions; N_f is the number of oscillator strengths for each ion, and σ_o (Mb) is the threshold photoionization cross section of each ion.

Ion	$N_{SL\pi}$	N_{bnd}	Singlet	Triplet	Quintet	N_f	σ_0
Si^0	27	218	${}^1S-{}^1I$	${}^3S-{}^3I$		3149	65.93
			${}^1P^o-{}^1I^o$	${}^3P^o-{}^3I^o$	${}^5S^o$		
S^{2+}	31	236	${}^1S-{}^1I$	${}^3S-{}^3I$	${}^5P-{}^5F$	3973	0.372
			${}^1P^o-{}^1H^o$	${}^3S^o-{}^3H^o$	${}^5S^o-{}^5D^o$		
Ar^{4+}	36	342	${}^1S-{}^1I$	${}^3S-{}^3I$	${}^5P-{}^5H$	7863	0.820
			${}^1P^o-{}^1H^o$	${}^3S^o-{}^3H^o$	${}^5S^o-{}^5G^o$		
Ca^{6+}	40	497	${}^1S-{}^1I$	${}^3S-{}^3I$	${}^5S-{}^5H$	16961	0.627
			${}^1P^o-{}^1H^o$	${}^3S^o-{}^3I^o$	${}^5S^o-{}^5I^o$		

The diagonalization of the Hamiltonian matrix is carried out for each $SL\pi$ independently and the bound states of the (e+ion) system correspond to negative eigenvalues. These are then assigned spectroscopic level identifications, in terms of the dominant configuration, primarily by analysing quantum defects along Rydberg series for the various angular momenta. A number of *positive* eigenvalues are also obtained on Hamiltonian diagonalization. These correspond to bound states that lie above the ionization limit but are forbidden to autoionize in pure LS coupling. The positive eigenvalue states are not considered in radiative calculations. Dipole oscillator strengths are computed for all transitions between the negative eigenvalue states allowed by the selection rules.

For photoionization calculations, the free electron wavefunctions are obtained at a fine mesh of positive energies. Autoionizing resonance structures in the photoionization cross sections are delineated at a mesh in effective quantum number ν, rather than the energy, since the resonance patterns are repeated when ν is incremented by unity. Thus a ν-mesh with a constant $\Delta\nu$ ensures a fixed number of points in each interval $(\nu, \nu+1)$ even as the resonances get narrower in terms of energy with increasing ν. In most of the OP work, resonances have been resolved up to an effective quantum number $\nu = \nu_{max} = 10.0$, using $\Delta\nu = 0.01$ (i.e. 100 points in each interval of 1.0 in ν). The small energy region below an excited target threshold, corresponding to $10.0 \le \nu \le \infty$, contains closely spaced narrow resonances which are averaged over using the Gailitis averaging procedure described by Yu and Seaton (1987). If more than one of the target states lie close to each other such that they have overlapping Gailitis averaging

regions, the states are treated as degenerate. For example, $3p^3\ ^2D^\circ$ and $^4S^\circ$ states of Ca^{7+} lie very close to each other (table 1) and hence are treated as degenerate in the photoionization calculation for Ca^{6+}.

4. Results

4.1. Energy levels

Almost all the bound states in *LS* coupling of Si^0, Si^{2+}, Ar^{4+} and Ca^{6+} with $n \le 10$ are obtained and identified. Table 3 shows the number of pure bound states (N_{bnd}) with $n \le 10$ and $l \le 5$, and corresponding $SL\pi s$, for the four ions. The number of bound states increases as the ion charge increases, N_{bnd} being 218 for neutral Si^0 going up to 497 for Ca^{6+}.

Calculated energies are compared with available observed energies in table 4. With very few exceptions the agreement of the present calculated energy values with the observed values is very good in general for all the four ions, usually within 1%. The exceptions, from among the large number of bound states, are: the $3s3p^3\ ^5S^\circ$ state of Si^0 (6%) and a few highly excited states, for example, $3p8s\ ^1P^\circ$, $3p9s\ ^1P^\circ$ and $3p9d\ ^3F^\circ$ that show larger discrepancies. For S^{2+}, the calculated energies are within 3% of the observed energies. For calculated A^{4+} energies the largest difference is 2.1% for $3p3d\ ^1P^\circ$, and for Ca^{6+} the maximum discrepancy is 2% compared to the observed energies.

4.2. Oscillator strengths

Before the OP, relatively few accurate calculations were carried out for radiative atomic parameters of importance in astrophysics and laboratory plasmas. In the present work we obtain a large number of oscillator strengths, for dipole allowed transitions in *LS* coupling, for the four elements of the Si sequence. While table 3 shows the total number of oscillator strengths obtained for each ion, comparisons of present oscillator strengths with other calculated and the observed values are made in table 5. Both the length, f_L, and the velocity, f_V, forms of the oscillator strengths are presented. Agreement between the two forms is in general a measure of the accuracy of the wavefunctions of the initial and the final states. In the *R*-matrix calculations the wavefunctions in the asymptotic region, outside the *R*-matrix boundary, are better represented. Although the length and velocity formulations generally agree well (e.g. Yu and Seaton 1987, Luo *et al* 1988), the former are somewhat more reliable in terms of accuracy. The level of agreement between the two is usually a few per cent; for A^{4+} and Ca^{6+} the agreement is better than for Si^0 and S^{2+}.

The present Si^0 oscillator strengths are compared in table 5 with the six-state CC calculation of Mendoza and Zeippen (1988), and two sets of measured values (O'Brian and Lawler 1991, Becker *et al* 1980). The few *f*-values computed by Mendoza and Zeippen compare reasonably well with our values. The present *f*-values compare quite well in general with those of O'Brian and Lawler (1991) measured using the recently developed technique of laser induced flourescence (with the exception of a weak transition $3p^2\ ^1D$–$3p3d\ ^1P^\circ$), usually within experimental uncertainties. Agreement of the present *f*-values with Becker *et al* is also good except for the same weak transition. Present calculations for oscillator strengths for very weak transitions may not be very accurate. Iglesias and Rogers (1992) have carried out atomic structure calculations using a parametric potential which does not explicitly include electron correlation

Table 4: Comparison of calculated energies (cal) of bound states of Si^0, S^{2+}, Ar^{4+} and Ca^{6+} (where the negative sign has been omitted for convenience) with the observed (obs) ones. The observed energies are from Martin and Zalubus (1983) and with a dot at the end from the compilation by Moore (1949) for Si^0, from Johansson *et al* (1992) except $^5S^o$ which is from Martin *et al* (1990) for S^{2+}, from Kelly (1987) for A^{4+}, and from Sugar and Corliss (1985) for Ca^{6+}. All energies in Ryd.

State	obs	cal	state	obs	cal	State	obs	cal
				Si^0				
$3p^2\,^3P$	0.598 55	0.6013	$3p5p\,^3D$	7.974 (−2)	7.980 (−2)	$3p5f\,^3G$	3.819 (−2)	4.026 (−2)
$3p^2\,^1D$	0.542 52	0.5433	$3p5p\,^3P$	7.683 (−2)	7.642 (−2)	$3p5f\,^1D$	3.787 (−2)·	3.993 (−2)
$3p^2\,^1S$	0.459 63	0.4543	$3p4d\,^3F^o$	7.604 (−2)	7.749 (−2)	$3p7s\,^3P^o$	3.680 (−2)·	3.820 (−2)
$3s3p^3\,^5S^o$	0.296 23	0.3159	$3p5p\,^3S$	7.556 (−2)	7.629 (−2)	$3p7s\,^1P^o$	3.528 (−2)	3.731 (−2)
$3p4s\,^3P^o$	0.236 69	0.2376	$3p5p\,^1D$	7.322 (−2)	7.282 (−2)	$3p6d\,^3P^o$	3.521 (−2)·	3.695 (−2)
$3p4s\,^1P^o$	0.226 37	0.2255	$3p5p\,^1S$	6.854 (−2)	6.766 (−2)	$3p6d\,^1D^o$	3.350 (−2)	3.430 (−2)
$3s3p^3\,^3D^o$	0.187 08	0.1981	$3p4d\,^1P^o$	6.408 (−2)	6.422 (−2)	$3p6d\,^3F^o$	3.094 (−2)	3.197 (−2)
$3p4p\,^1P$	0.169 03	0.1670	$3p4f\,^1F$	6.360 (−2)·	6.428 (−2)	$3p6d\,^1P^o$	2.886 (−2)	2.840 (−2)
$3p3d\,^1D^o$	0.168 42	0.1764	$3p4f\,^3F$	6.252 (−2)·	6.425 (−2)	$3p6f\,^3F$	2.811 (−2)·	2.831 (−2)
$3p4p\,^3D$	0.161 04	0.1591	$3p4d\,^1F^o$	6.324 (−2)	6.410 (−2)	$3p6d\,^1F^o$	2.762 (−2)·	2.820 (−2)
$3p4p\,^3P$	0.152 23	0.1478	$3p4d\,^3D^o$	6.157 (−2)	6.297 (−2)	$3p6d\,^3D^o$	2.691 (−2)	2.818 (−2)
$3p4p\,^3S$	0.149 76	0.1482	$3p4f\,^3G$	6.115 (−2)·	6.288 (−2)	$3p8s\,^3P^o$	2.631 (−2)·	2.671 (−2)
$3p3d\,^3F^o$	0.144 60	0.1504	$3p4f\,^3D$	6.015 (−2)·	6.224 (−2)	$3p8s\,^1P^o$	2.390 (−2)·	2.618 (−2)
$3p4p\,^1D$	0.142 56	0.1378	$3p4f\,^1D$	6.053 (−2)·	6.221 (−2)	$3p7d\,^1D^o$	2.257 (−2)	2.443 (−2)
$3p3d\,^3P^o$	0.139 42	0.1454	$3p6s\,^3P^o$	5.793 (−2)·	5.916 (−2)	$3p7d\,^3F^o$	2.233 (−2)	2.300 (−2)
$3p4p\,^1S$	0.129 60	0.1239	$3p6s\,^1P^o$	5.574 (−2)·	5.750 (−2)	$3p7d\,^1P^o$	2.138 (−2)	2.081 (−1)
$3p3d\,^1F^o$	0.113 65	0.1170	$3p5d\,^3P^o$	5.277 (−2)·	5.462 (−2)	$3p7d\,^1F^o$	1.997 (−2)	2.068 (−2)
$3p3d\,^1P^o$	0.113 42	0.1154	$3p5d\,^1D^o$	5.042 (−2)·	5.164 (−2)	$3p7d\,^3D^o$	1.947 (−2)	2.071 (−2)
$3p3d\,^3D^o$	0.105 78	0.1093	$3p5d\,^3F^o$	4.630 (−2)	4.743 (−2)	$3p9s\,^1P^o$	1.703 (−2)	1.938 (−2)
$3p5s\,^3P^o$	0.103 96	0.1042	$3p5d\,^1P^o$	4.126 (−2)	4.100 (−2)	$3p8d\,^1D^o$	1.679 (−2)	1.829 (−2)
$3p5s\,^1P^o$	9.990 (−2)	0.1005	$3p5f\,^1D$	4.055 (−2)·	3.991 (−2)	$3p8d\,^3F^o$	1.666 (−2)	1.734 (−2)
$3p4d\,^1D^o$	8.502 (−2)	8.640 (−2)	$3p5f\,^3F$	4.053 (−2)·	4.089 (−2)	$3p8d\,^1P^o$	1.652 (−2)	1.590 (−2)
$3p4d\,^3P^o$	8.324 (−2)	8.557 (−2)	$3p5d\,^1F^o$	4.019 (−2)	4.075 (−2)	$3p8d\,^1F^o$	1.500 (−2)	1.581 (−2)
$3p5p\,^1P$	8.250 (−2)	8.228 (−2)	$3p5d\,^3D^o$	3.931 (−2)	4.050 (−2)	$3p9d\,^3F^o$	1.296 (−2)	1.354 (−2)
				S^{2+}				
$3p^2\,^3P$	2.573 53	2.574	$3p4s\,^3P^o$	1.234 32	1.219	$3p4p\,^1S$	0.908 11	0.8996
$3p^2\,^1D$	2.470 35	2.469	$3p3d\,^3D^o$	1.227 68	1.209	$3p4d\,^1D^o$	0.704 09	0.6855
$3p^2\,^1S$	2.326 01	2.308	$3p4s\,^1P^o$	1.221 29	1.213	$3p4d\,^3F^o$	0.703 92	0.6891
$3s3p^3\,^5S^o$	2.038 87	2.071	$3p3d\,^1D^o$	1.188 60	1.156	$3p4d\,^3D^o$	0.689 41	0.6684
$3s3p^3\,^3D^o$	1.807 46	1.824	$3p3d\,^1F^o$	1.137 28	1.116	$3p4d\,^3P^o$	0.678 10	0.6610
$3s3p^3\,^3P^o$	1.673 60	1.674	$3p3d\,^1P^o$	1.077 77	1.030	$3p5s\,^3P^o$	0.656 78	0.6452
$3s3p^3\,^1D^o$	1.624 37	1.630	$3p4p\,^1P$	1.046 68	1.046	$3p4d\,^1F^o$	0.649 40	0.6291
$3p3d\,^3F^o$	1.457 18	1.454	$3p4p\,^3D$	1.021 99	1.021	$3p5s\,^1P^o$	0.647 76	0.6377
$3s3p^3\,^1P^o$	1.326 52	1.293	$3p4p\,^3P$	0.997 08	0.9961	$3p4d\,^1P^o$	0.627 59	0.6172
$3s3p^3\,^3S^o$	1.315 37	1.281	$3p4p\,^3S$	0.987 58	0.9864			
$3p3d\,^3P^o$	1.269 33	1.262	$3p4p\,^1D$	0.960 73	0.9573			
				Ar^{4+}				
$3p^2\,^3P$	5.514 71	5.499	$3s3p^3\,^1D^o$	4.109 44	4.109	$3p3d\,^1F^o$	3.279 28	3.230
$3p^2\,^1D$	5.366 17	5.355	$3s3p^3\,^3S^o$	3.769 29	3.721	$3p3d\,^1P^o$	3.217 13	3.149
$3p^2\,^1S$	5.169 22	5.128	$3s3p^3\,^1P^o$	3.734 49	3.686	$3p4s\,^3P^o$	2.807 28	2.751
$3s3p^3\,^3D^o$	4.405 42	4.424	$3p3d\,^3P^o$	3.528 76	3.492	$3p4s\,^1P^o$	2.769 06	2.705
$3s3p^3\,^3P^o$	4.222 83	4.223	$3p3d\,^3D^o$	3.468 49	3.430			
				Ca^{6+}				
$3p^2\,^3P$	9.388 58	9.364	$3s3p^3\,^1D^o$	7.556 28	7.545	$3p3d\,^1F^o$	6.451 19	6.383
$3p^2\,^1D$	9.212 52	9.187	$3s3p^3\,^3S^o$	7.176 97	7.123	$3p3d\,^1P^o$	6.372 68	6.303
$3p^2\,^1S$	8.965 41	8.927	$3s3p^3\,^1P^o$	7.110 91	7.064	$3p4s\,^1P^o$	4.867 43	4.780
$3s3p^3\,^3D^o$	7.950 53	7.963	$3p3d\,^3P^o$	6.794 80	6.738	$3p4s\,^3P^o$	4.922 13	4.839
$3s3p^3\,^3P^o$	7.722 28	7.718	$3p3d\,^3D^o$	6.716 12	6.660			

Table 5. Oscillator strengths or f-values for transitions in Si^0, S^{2+}, Ar^{4+} and Ca^{6+}. f_L and f_V are the calculated oscillator strengths in length and velocity forms respectively. MZ, Mendoza and Zeippen 1988; IR, Iglesias and Rogers (1992); HH, Ho and Henry (1987); EB, Biemont (1986).

Transition	Multiplet	f_L	f_V	f_L	f	f
				Si^0		
		(present)		MZ	IR	expt
$3p^2$–$3p3s$	^3P–$^3P°$	0.236	0.216	0.214	0.216	0.211[a]
	^1D–$^1P°$	0.195	0.180		0.193	0.162[a], 0.170[b]
	^1S–$^1P°$	0.101	0.085		0.140	0.0913[a], 0.098[b]
$3p^2$–$3p5s$	^3P–$^3P°$	0.029	0.028	0.033		
$3p^2$–$3p3d$	^3P–$^3P°$	0.053	0.054	0.042		0.0513[a]
	^3P–$^3D°$	0.269	0.244	0.296		
	^1D–$^1P°$	0.0056	0.0057			0.0029[a], 0.0036[b]
	^1D–$^1D°$	0.041	0.041			0.040[a]
	^1D–$^1F°$	0.358	0.334			0.282[a]
	^1S–$^1P°$	0.409	0.400			0.300[a], 0.355[b]
$3p^2$–$3p4d$	^3P–$^3P°$	0.012	0.009	0.020		
	^3P–$^3D°$	0.155	0.147	0.146		
$3p^2$–$3s3p^3$	^3P–$^3D°$	0.051	0.052	0.022		0.056[a]
$3p4s$–$3p4p$	$^1P°$–^1S	0.096	0.090		0.184	
	$^1P°$–^1P	0.360	0.343		0.240	
	$^1P°$–^1D	0.680	0.613		0.730	
	$^3P°$–^3S	0.121	0.121		0.145	
	$^3P°$–^3P	0.435	0.382		0.482	
	$^3P°$–^3D	0.622	0.574		0.649	
$3p4p$–$3p4d$	^1P–$^1D°$	0.530	0.547		0.043	
	^1P–$^1P°$	0.0075	0.0061		0.040	
	^3D–$^3F°$	0.396	0.410		0.108	
				S^{2+}		
		(present)		HH		expt
$3p^2$–$3s3p^3$	^3P–$^3D°$	0.024	0.021	0.022	0.025	0.022±0.002[c], 0.022[d]
	^3P–$^3P°$	0.043	0.038	0.034	0.050	0.036[d]
	^3P–$^3S°$	0.360	0.340	0.35	0.33	
	^1D–$^1P°$	0.38	0.37	0.37	0.33	
	^1D–$^1D°$	0.021	0.019	1.03	1.03	0.0167±0.0005[c], 0.99±0.10[f]
	^1S–$^1P°$	0.0023	0.0052	0.002	0.014	
$3p^2$–$3p3d$	^3P–$^3P°$	0.780	0.760	0.39	0.30	
	^3P–$^3D°$	1.670	1.630	1.86	1.62	0.96±0.19[e]
	^1D–$^1P°$	0.024	0.024	0.014	0.042	
	^1D–$^1D°$	1.02	0.982	0.107	0.027	
	^1D–$^1F°$	1.36	1.35	1.54	1.60	
	^1S–$^1P°$	2.71	2.64	2.74	2.91	
$3p4p$–$3p4d$	^3D–$^3F°$	0.947	0.880			0.685±0.05[e]
$3p^2$–$3p4s$	^3P–$^3P°$	0.087	0.083	0.57	0.51	
	^1D–$^1P°$	0.094	0.094	0.10	0.14	0.07±0.04[e]
	^1S–$^1P°$	0.066	0.062	0.064	0.101	0.08±0.05[e]

Table 5. (continued)

		Ar^{4+} (present)		expt
3p^2–3s3p^3	^{3}P–^{3}P^o	0.061	0.059	0.057±0.002^f
	^{3}P–^{3}S^o	0.306	0.300	
	^{3}P–^{3}D^o	0.042	0.041	
3p^2–3p3d	^{3}P–^{3}P^o	0.581	0.569	
	^{3}P–^{3}D^o	1.411	1.140	
	^{1}D–^{1}F^o	1.212	1.208	
	^{1}S–^{1}P^o	2.270	2.220	
3p^2–3p4s	^{3}P–^{3}P^o	0.147	0.143	

		Ca^{6+} (present)		EB
3p^2–3s3p^3	^{3}P–^{3}D^o	0.050	0.049	0.047
	^{3}P–^{3}P^o	0.067	0.064	0.064
	^{3}P–^{3}S^o	0.268	0.264	0.249
	^{1}D–^{1}P^o	0.250	0.246	0.236
	^{1}D–^{1}D^o	0.088	0.085	0.096
	^{1}S–^{1}P^o	0.175	0.166	0.191
3p^2–3p3d	^{3}P–^{3}D^o	1.133	1.133	1.082
	^{3}P–^{3}P^o	0.460	0.457	0.399
	^{1}D–^{1}D^o	0.678	0.674	0.504
	^{1}D–^{1}F^o	0.974	0.974	0.896
3p^2–3p4s	^{3}P–^{3}P^o	0.150	0.147	0.143
	^{1}D–^{1}P^o	0.141	0.137	0.133
	^{1}S–^{1}P^o	0.115	0.109	0.120

[a] O'Brian and Lawler (1991).
[b] Becker *et al* (1980).
[c] Berry *et al* (1970).
[d] Livingston *et al* (1976).
[e] Ryan *et al* (1989).
[f] Irwin *et al* (1973).

effects. Their oscillator strengths from the ground configuration agree with the present results, but significant differences are found for other transitions, especially for the 3p4p–3p4d transitions where differences range from 40% to up to an order of magnitude.

The calculated S^{2+} oscillator strengths show a better agreement between the length and velocity forms, except for the weak transition 3p^2 ^{1}S–3s3p^3 ^{1}P^o, than the atomic structure calculations by Ho and Henry (1987). The present *f*-values differ significantly from those of Ho and Henry for the transition 3p^2 ^{3}P–3p3d ^{3}P^o and ^{1}D–^{1}D^o transitions. Comparisons are also made with available experimental values using the beam-foil technique. The present values are somewhat higher than those measured by Berry *et al* (1970). Agreement of the present calculated *f*-values is reasonably good with those of Livingston *et al* (1976) and Ryan *et al* (1989) except for the transition 3p^2 ^{3}P–3p3d ^{3}D^o. The measured value for a single transition by Irwin *et al* (1973) lies much higher than the present value, as well as that by Berry *et al*.

Oscillator strengths for some transitions of A^{4+} are presented in table 5. Only one published measured value has been found. The present oscillator strengths appear to be the first calculated values. The single measured transition (Irwin *et al* 1973) by the

beam-foil technique agrees well the calculated value. The present f-values should be of good accuracy since the difference between the length and velocity forms is found to be very small.

Some oscillator strengths of Ca^{6+} are presented in table 5 and compared with the atomic structure calculations by Biemont (1986), who included some relativistic effects. The parameters in his model were adjusted to reproduce the observed energy values. Our results agree well with those listed by Biemont. The present f_L and f_V values also agree with each other to about 5%.

4.3. Total and partial photoionization cross sections

Detailed photoionization cross sections which include autoionizing resonances through interchannel couplings are calculated for all calculated bound states of Si^0, S^{2+}, Ar^{4+} and Ca^{6+} as quoted in table 3. The Rydberg series of autoionizing resonances arise from the $(N+1)$-electron quasi-bound states of the type $(S_t L_t \pi_t)nl$, where $S_t L_t \pi_t$ are the various states of the target ion included in the CC expansion.

Illustrative results are presented for some of the important states, in particular the ground and the metastable states: ^3P, ^1D and ^1S. In addition, we describe in detail two other significant features of the present calculations: (i) partial photoionization cross sections, with the residual ion in an excited state, and (ii) an important type of resonances known as photoexcitation-of-core (PEC) resonances, first discussed by Yu and Seaton (1987), that manifest themselves strongly in the photoionization of excited bound states in a Rydberg series.

4.3.1. Total cross sections.
The total photoionization cross sections for the ground state of Si-like ions are presented in figure 1. The threshold photoionization cross section, σ_0, for the ground state ^3P of each ion is given in table 3. σ_0 for Si^0 shows a large value compared with the other three ions indicating a strong resonance at the threshold. The presence of a large and wide resonance spanning more than an order of magnitude in the ^3P photoionization cross section can be observed from the detailed plots in figure 1(a). The same resonance at the threshold is observed in the work by Mendoza and Zeippen (1988). The bottom panels of figures 1(b), (c) and (d) show similar plots of the ^3P ground state of the other three elements. All cross sections show extensive resonance structures throughout the range of energies from the ionization threshold up to the highest target threshold considered. These resonances form from the bound channel states and autoionizing states of Rydberg series belonging to the target states and enhance the background cross sections significantly. The Rydberg nature of the resonances is evident from the patterns that are seen to converge on to the various target states; the most easily discernable is the first excited state ^4P of the residual ion.

In the ground state photoionization cross sections in the lowest panels of figure 1, the circles correspond to cross sections calculated in the central field approximation (Reilman and Manson 1979). For neutral silicon, the central field approximation underestimates the background cross sections significantly, by about a factor of two and a half near threshold to a factor of four at higher energy. For S^{2+}, it overestimates the threshold cross sections by 50% and falls by about a factor of two in the high energy region. The comparison for Ar^{4+} in figure 1(c) may be difficult because the first circle corresponds to their near threshold cross section as tabulated, not at a higher photoelectron energy. This cross section in the central field approximation is about
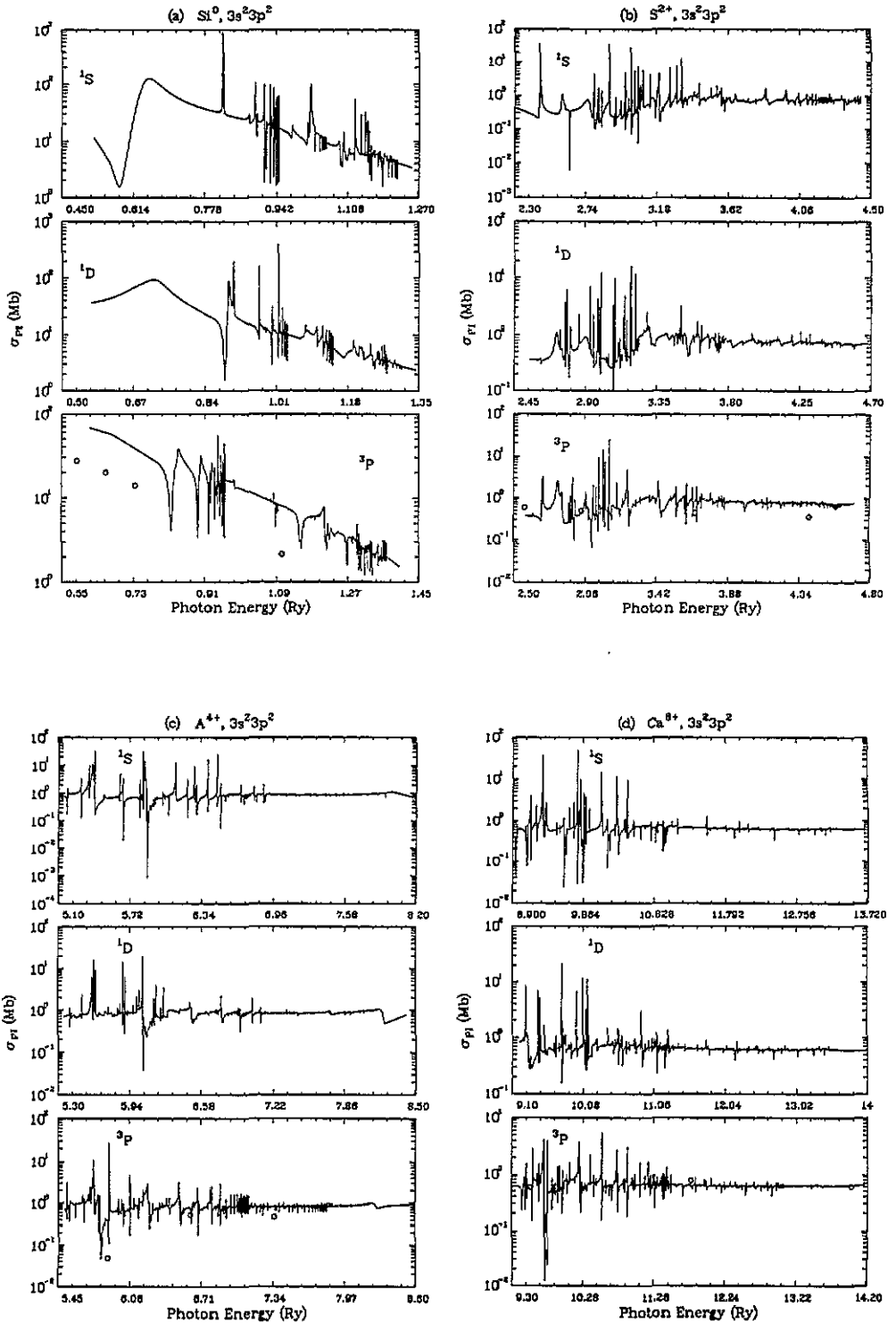
Figure 1. Photoionization cross sections of ground ^3P and metastable ^1D, ^1S states of the ground configuration $3s^23p^2$ of (a) Si^0, (b) S^{2+}, (c) Ar^{4+}, (d) Ca^{6+}.

twenty times lower from the present calculations. Their cross sections rise at higher energy but stay about 40% below the average background cross sections of the present work. The central field approximation agrees well with our R-matrix results only for Ca^{6+}, the most highly charged ion considered in the present work.

Unlike the central field approximation, which does not take into account channel couplings, a simple Z-dependent variation for σ_0 of the elements of the Si sequence cannot be obtained because of the enhancement and variations in the background cross sections at and near threshold region by the autoionizing resonances. The same is true of many other detailed close coupling calculations of photoionization which include autoionization effects (e.g. the carbon sequence (Nahar and Pradhan 1991)). This is discussed further later.

The upper two panels of figure 1 show the total photoionization cross sections of the metastable states ^{1}D and ^{1}S dominated by the ground configuration $3s^23p^2$ of Si^0, S^{2+}, Ar^{4+} and Ca^{6+}. Metastable states are of considerable practical importance since they are unable to decay to the ground state via dipole transitions and consequently have long lifetimes. A significant fraction of the level population in experimental beams or laboratory or astrophysical plasmas may be present in metastable states. For Si^0, each state of the ground configuration shows the presence of a large resonance near the threshold in figure 1(a). Si^0 cross sections behave differently from the other three ions in terms of the large cross section near the threshold and in the background variations for all three lowest states. In the case of S^{2+}, Ar^{4+} and Ca^{6+} the resonance structures in the states dominated by the ground configuration are different for each ion though the average magnitude of the background cross sections of the metastable states remains in the same range as that for the ^{3}P ground state.

4.3.2. Partial photoionization cross sections. Partial photoionization cross section of atoms and ions into various excited states of the residual ion are important astrophysically for the determination of level populations in these states under conditions of non-LTE. Partial photoionization cross sections of the $3s^23p^2$ ^{3}P ground state of Si^0, S^{2+}, Ar^{4+} and Ca^{6+}, leaving the residual ion in the ground and various excited states (as given in table 1), are obtained and presented in figures 2(a)–(d). The bottom panels show the total, that is the sum of the partial cross sections, while the upper panels correspond to partial photoionization cross sections leaving the residual ion in various excited states, as specified in each panel in figure 2. For Ca^{6+}, the upper two panels specify more than one target state which means that those panels correspond to the combined cross sections for those states. The reason for this is that these target states lie very close to each other and have been treated as degenerate. In these figures arrows point to the threshold energies of the target states with respect to the ground level. Slight differences in the resolution and resonance positions in photoionization cross sections for the ^{3}P ground state of Si^0 and S^{2+} can be noticed in the bottom panels of figures 1 and 2. These are due to the use of calculated target energies in figure 1, and observed target energies for the partial photoionization cross sections; the two sets of energies are, as pointed out earlier with table 1, very close to each other.

From figure 2 it can be seen that the photoionization into the ^{2}P^o ground state of the residual ion dominates the process and the other partial cross sections contribute relatively small amounts to the total background. The important feature to be noticed is the extensive autoionizing resonance structure in most of the partial cross sections, often at or in the near threshold region. Each resonance may correspond to a high probability for a line formation at a given frequency. Determination of the branching
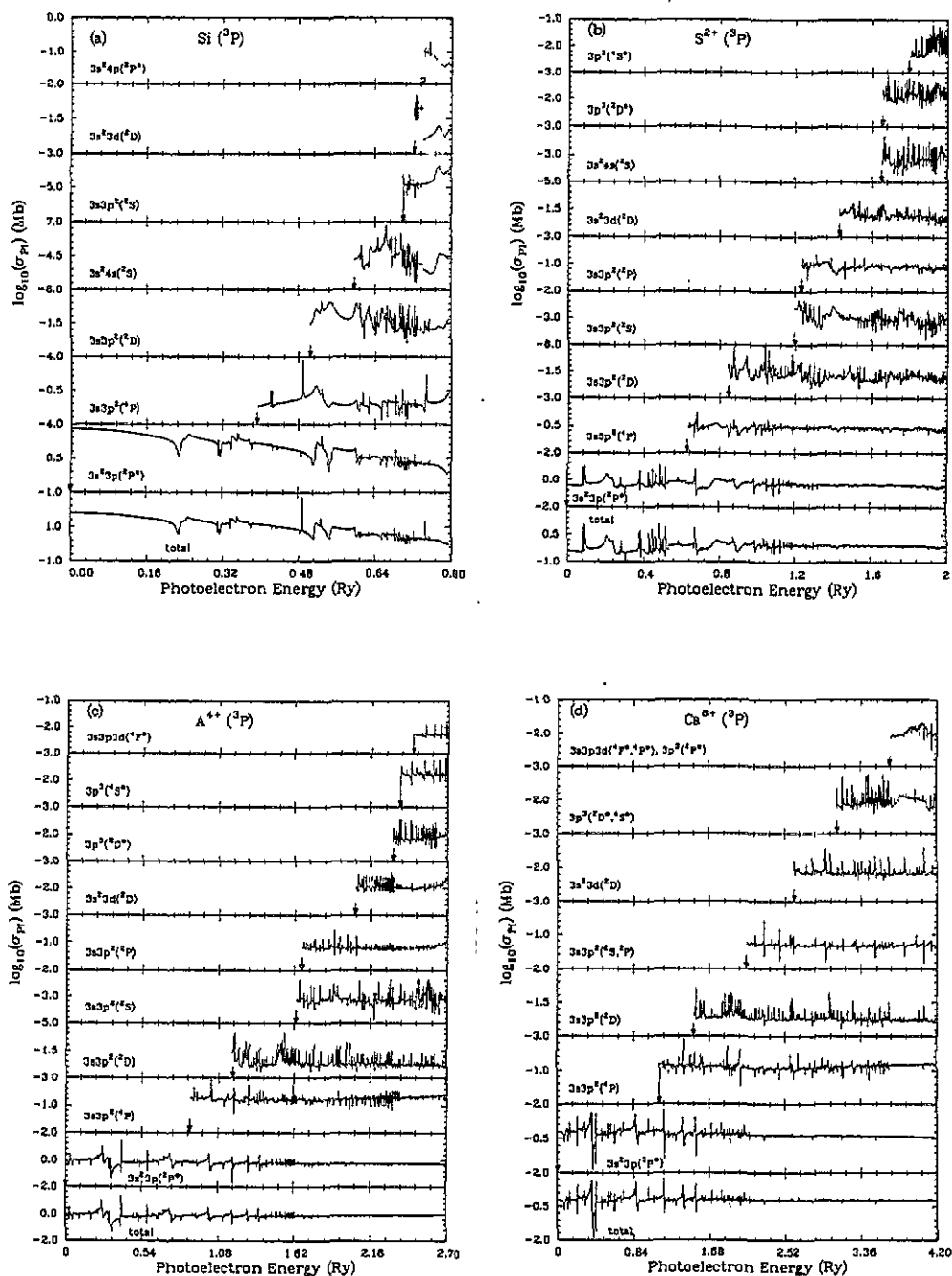
Figure 2. (*a*) Partial photoionization cross sections of $3s^2 3p^2$ ^3P ground state of Si^0. The bottom panel shows the total cross section and the upper panels partial cross sections leaving the residual Si^+ in particular core states as specified in the panels. The arrows point at the threshold cross sections. The upper limit of the panels are not specified except for the top panel. (*b*) Same as figure (*a*) except for S^{2+}. (*c*) Same as (*a*) except for Ar^{4+}. (*d*) Same as (*a*) except for Ca^{6+}.

ratios of these partial cross sections at *ionization thresholds* may not be obtained accurately because of the resonances (see Nahar and Pradhan 1992).

4.3.3. z dependence. As shown in table 3, for the Si sequence ions there appears to be no systematic trend in threshold cross sections, σ_0, with ion charge $z = Z - N$, as usually obtained in simpler approximations such as the central field approximation. Figure 3 shows z-scaled photoionization cross sections of the ^3P ground state of the four Si-like ions. The slight differences in the resolution and the resonance positions of ground state photoionization cross sections of Si^0 and S^{2+} between figures 1 and 3 are due to the use of calculated and observed target energies, as explained in the above section for partial photoionization. The purpose of figure 3 is to examine an overall z dependence of the cross sections. It was found by Nahar and Pradhan (1992) for the carbon sequence ions that even though no generally precise z dependence can be obtained for individual cross sections, the background on the whole did show some z dependence for the different elements of the C-isoelectronic sequence, especially for the more highly charged members.

For the Si-sequence ions although we find no discernible z dependence for Si^0 and S^{2+}, for Ar^{4+} and Ca^{6+} the value of $lg[z^2\sigma_{PI}]$ is about 1.4 for both ions, indicative of a similar charge dependence of the background cross sections for all other higher members of the sequence (as in Nahar and Pradhan 1992). For S^{2+}, the value of $lg[z^2\sigma_{PI}]$ is about 0.8, while for Si^0 an average background value cannot be obtained
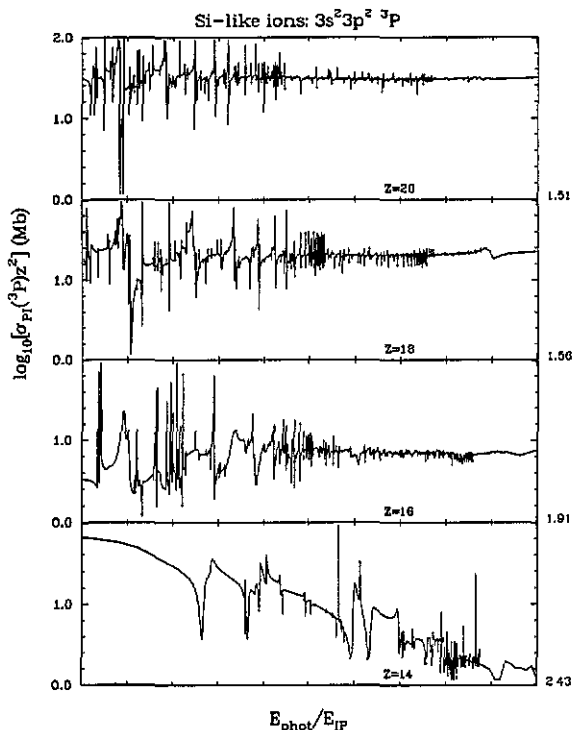

Figure 3. z-scaled photoionization cross sections of Si like ions: Si^0, S^{2+}, Ar^{4+} and Ca^{6+}. The energy axis in each panel is scaled by the ionization energy of the corresponding ion and the energy range goes from 1.0 to the value printed on the bottom right of each panel. The upper limit of the panels is not specified for the top panel.

due to the presence of large resonance structures. Si^0 is a complex neutral system with a number of electrons and the correlation effects are more involved than in the other members of the sequence. It might be emphasized that while the resonances appear narrower for highly charged ions due to the energy scale that increases as z^2, the autoionization rates themselves are independent of ion charge and therefore the relative importance of resonances in photoionization cross sections persists even for the higher members of an isoelectronic sequence. This fact may be important in practical applications where the photon frequency dependence in a given energy region needs to be considered, usually in the near threshold region.

4.3.4. Photoionization of excited states. Photoionization of excited bound states with $n \le 10$ and $l \le 5$ for the active electrons is considered. The number of bound states N_{bnd} in table 3 corresponds to the total number of states for which photoionization cross sections have been calculated. These results have been used in the calculation of stellar opacities and are also being utilized in the calculation of total electron–ion recombination rate coefficients, as discussed by Nahar and Pradhan (1991, 1992).

There are two prominent features exhibited by the detailed excited state photoionization cross sections. First, all the excited states show the presence of a large number of autoionizing resonances (e.g. metastable states in figure 1) and consequently no smooth fitting procedure can be formulated. Most of the Rydberg excited states, in addition to narrow resonances, show large wide resonances known as PEC (photoexcitation-of-core) resonances, at energies corresponding to strong dipole transitions in the core ion, usually from the ground state. The outer electron in the Rydberg state remains a 'spectator' as in the dielectronic recombination process, PECs are more prominent in highly excited states where the valence electron is far removed and is weakly coupled to the core states. Figure 4 shows the wide PEC resonances in the photoionization cross sections of $3s^2 3pnd$ $^1F^o$ series of excited states of Si^0, n ranging from 4 to 11, corresponding to dipole allowed Si^+ core transitions $3s^2 3p$ $^2P^o \rightarrow 3s3p^2$ (^2D, ^2S, ^2P), $3s^2 3d$ ^2D, $3s^2 4s$ ^2S. As we go up high in the excited nd series of states, PECs become more and more prominent, located at photon energies corresponding to the transition energy between the core states mentioned above. The series show a monotonic decrease of cross sections in the low energy region similar to cross sections calculated in the hydrogenic or central field approximation, but at higher energies the cross sections are considerably enhanced as PEC resonances begin to manifest themselfes. This appears to be one of the crucial differences between photoionization calculations in the CC approximation and the simpler approximations that provide only the background cross sections and are therefore likely to severely underestimate the *effective* cross sections. It can be noticed that the enhancement due to PEC resonances can be such that the effective cross sections at higher energies may even be greater than the cross section value at the first ionization threshold.

The second important effect of interchannel coupling is that photoionization may occur through autoionizing channels at energies below the ionization threshold of the optical electron. Figure 5 shows the photoionization of the $3s3p^3$ $^3S^o$ excited state of S^{2+} with energy range going up to the highest excited state considered in the CC expansion of target S^{3+}. Figure 5(a) plots the total cross sections with positions of various target states shown by arrows and figure 5(b) shows an expanded version of the region between $^2P^o$ and ^4P. The threshold for ionization of the 3p optical electron of the $^3S^o$ state corresponds to the residual or target ion $3s3p^2$ ^4P state. Therefore, excluding interchannel coupling would result in a zero cross section below this
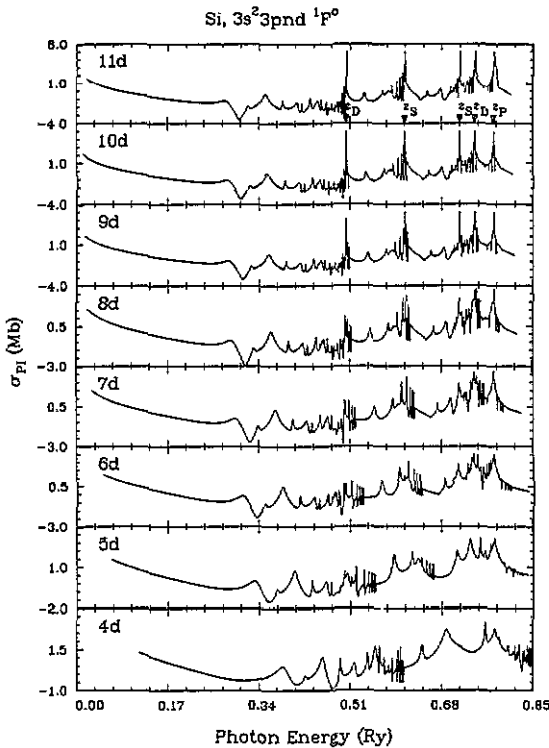
Si, $3s^2 3pnd\ ^1F^\circ$

Figure 4. Photoionization cross sections of Rydberg series of states $3s^2 3pnd\ ^1F^\circ$, $4 \leqslant n \leqslant 11$, of Si^0 illustrating the PEC resonances due to five dipole allowed core transitions: $3s^2 3p^2 P^0 \rightarrow 3s3p^2\ (^2D, ^2S, ^2P)$, $3s^2 3d\ ^2D$, $3s^2 4s\ ^2S$. The upper limit of the panels is not shown except for the top panel.

threshold. On the other hand the effective cross section, although entirely due to autoionization, is quite large as it is dominated by large autoionizing resonances (figure 5). The resonances of the ^4P np series are identified in figure 5. The wide ^4P $5p$ resonance above the $^2P^\circ$ ground state of S^{3+} shows a rise by several orders of magnitude.

5. Conclusion

Extensive close coupling calculations for the radiative data, energy levels, oscillator strengths and photoionization cross sections corresponding to a large number of bound states have been carried out for the four ions Si^0, S^{2+}, Ar^{4+} and Ca^{6+} in the silicon sequence. Calculations for Fe^{12+} have been carried out by Mendoza (1992), also as part of the OP, and will be reported independently. Estimates of uncertainties in computed energies and f-values can be inferred from detailed comparisons with the experimental values that are given. As there are very few measurements for photoionization cross sections, it is difficult to assess the uncertainties in general but we estimate these to be at the level of 10%, based on the accuracy of the energies and the f-values. The calculated oscillator strengths and energy levels agree quite well with available measured values and previous calculations of high accuracy. Partial photoionization cross sections of the ground state of each ion are presented. The z-scaled behaviour of photoionization cross sections of the sequence is studied and found to have some
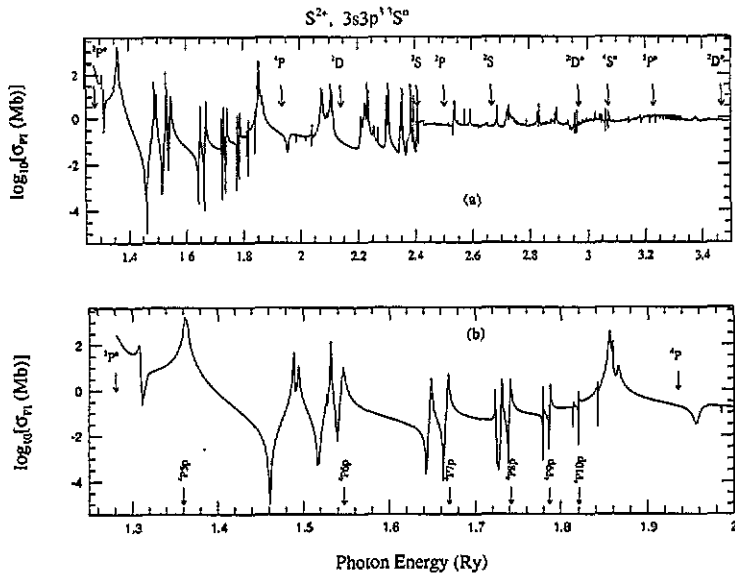
Figure 5. Photoionization of the $3s3p^3 \, ^3S^\circ$ state of S^{2+}. The top part shows the total cross sections up to the highest excited target state of S^{3+} where arrows point to positions of various target states. The bottom part shows the expanded region between $^2P^\circ$ and ^4P where photoionization proceeds through autoionizing channels only. The autoionizing resonances of the ^4P np series are shown by arrows.

uniform dependence for the background cross sections for Ar^{4+} and Ca^{6+}. To our knowledge this work reports the first calculation of Ar^{4+} oscillator strengths and detailed photoionization cross sections of S^{2+}, Ar^{4+} and Ca^{7+}.

References

Becker U, Kerkhoff H, Kwiatkowski M, Schmidt M, Teppner U and Zimmermann P 1980 *Phys. Lett.* **76A** 125
Berrington K A, Burke P G, Butler K, Seaton M J, Storey P J, Taylor K T and Yu Yan 1987 *J. Phys. B: At. Mol. Phys.* **20** 6379
Berry H G, Schectman R M, Martinsen I, Bickel W S and Bashkin S J 1970 *J. Opt. Soc. Am.* **60** 335
Biemont E 1986 *J. Opt. Soc. Am.* B 3, 163
Buchet-Poulizac M C, Buchet J P and Ceyzeriat P 1982 *Nucl. Instrum. Methods* **202** 13
Eissner W, Jones M and Nussbaumer H 1974 *Comput. Phys. Commun.* **8** 270
Ho Y K and Henry R J 1987 *Phys. Scr.* **35** 831
Iglesias C A and Rogers F J 1992 *Rev. Mex. Astron. Astrofis.* **23** 9
Irwin D J G and Livingston A E 1976. *Can. J. Phys.* **54** 805
Irwin D J G, Livingston A E and Kernahan J A 1973 *Nucl. Instrum. Methods* **110** 111

Johansson L, Magnusson C E, Joelsson I, Zetterberg P O 1992 *Phys. Scr.* in press (their relative energies have been scaled with respect to the ionization energy)

Kelly R L 1987 Unpublished compilation, closely corresponds to Kelly R L 1987 *J. Phys. Chem. Ref. Data* **16** Suppl. 2 (private communication with NIST)

Livingston A E, Dumont P D, Baudinet-Robinet Y, Garnir H P, Biemont E and Grevesse N 1976 *Beam-Foil Spectroscopy* ed I A Sellin and D J Pegg (New York: Plenum) p 339

Livingston A E, Pinnington E H, Irwin D J G, Kernahan J A and Brooks R L 1981 *J. Opt. Soc. Am.* **71** 442

Luo D, Pradhan A K and Shull J M 1988 *Astrophys. J.* **335** 598

Martin W C and Zalubas R 1983 *J. Phys. Chem. Ref. Data* **12** 323

Martin W C, Zalubus R and Musgrove A 1990 *J. Phys. Chem. Ref. Data* **19** 821

Mendoza C 1992 private communication

Mendoza C and Zeippen C J 1988 *J. Phys. B: At. Mol. Opt. Phys.* **21** 259

Moore C E 1949 *Atomic Energy Levels*, NBS CCircular No 467 (Washington DC: US Govt Printing Office)

Morton D C 1978 *Astrophys. J.* **222** 863

Nahar S N and Pradhan A K 1991 *Phys. Rev.* A **44** 2935

—— 1992 *Phys. Rev.* A **45** 7887

O'Brien T R and Lawler J E 1991 *Phys. Rev.* A **44** 7134

Reilman R F and Manson S T 1979 *Astrophys. J. Suppl.* **40** 815

Reistad N and Engstrom L 1988 *Zstrophys J.* **327** 502

Ryan L J, Rayburn L A and Cunningham A J 1989 *J. Quant. Spectrosc. Radiat. Transfer* **42** 295

Seaton M J 1987 *J. Phys. B: At. Mol. Phys.* **20** 6363

Shulz-Gulde E 1969 *J. Quant. Spectrosc. Radiat. Transfer* **9** 13

Sugar J and Corliss C 1985 *J. Phys. Chem. Ref. Data* **14** Suppl. 2

Yu Y and Seaton M J 1987 *J. Phys. B: At. Mol. Phys.* 6409